SUPPORTING INFORMATION

Supramolecular Enhancement of Protein Analysis via the Recognition of Phenylalanine with Cucurbit[7]uril

Jong Wha Lee,[†,‡,⊥] *Min Hyeon Shin,*[†,⊥] *William Mobley,*[§] *Adam R. Urbach,*[*,§] *and Hugh I. Kim*[*,‡]

[†]Department of Chemistry, Pohang University of Science and Technology (POSTECH), Pohang, 37673, South Korea

[‡]Department of Chemistry, Korea University, Seoul, 02841, South Korea

[§]Department of Chemistry, Trinity University, San Antonio, Texas 78212, United States

[⊥]These authors contributed equally to this work

[*]To whom correspondence should be addressed: E-mail: aurbach@trinity.edu, hughkim@korea.ac.kr

Table of contents

Fragmentation Pathways of Model Peptides. To characterize the fragmentation pathways of cucurbit[7]uril (CB[7])-bound peptides, we performed tandem mass spectrometry (MS) of two model peptides with N-terminal Phe or Lys: Phe-Gly-Gly-Gly-Gly (FGGGG) and Lys-Gly-Gly-Gly-Gly (KGGGG). Although the binding affinity of Lys to CB[7] is much lower than that of Phe in solution, the CB[7] complex of Lys has good stability in the gas phase.[1] We added the KGGGG peptide for investigation because the additional basic site at the N-terminus of the peptide may provide further insights into the fragmentation pathways.

ESI of the CB[7] complex of the model peptides produced both singly charged and doubly charged forms of the ions (Figure S9). Collision-induced dissociation (CID) of the complex ions generated both b and y ions with CB[7] from the singly charged forms, whereas no y ions with CB[7] were generated from the doubly charged forms. The formation of y ions with CB[7] is particularly interesting because it shows not only that migration of CB[7] has occurred,[2] but also that the migration occurred specifically during the CID process. This follows because there are no functional groups in y ions except the charged N-terminal amine that can stably bind to CB[7], and the charged N-terminal amine is formed during the CID process.

The large sizes of the CB[7]•peptide complex ions prohibit us from performing theoretical calculations to elucidate their fragmentation pathways. However, fragmentation pathways of peptide ions have been studied extensively, and these studies provide clues to the dissociation mechanism of our ions.[3] The ‘mobile proton’ theory is now generally accepted to explain peptide fragmentation pathways.[4] According to this theory, protons are localized initially at the most basic sites within peptides, and they migrate to the less basic sites upon activation. Migration of a

proton to the amide backbone and subsequent nucleophilic attack at the amide carbon generates b and y fragment ions. In the absence of side chain nucleophiles, the nucleophilic attack can proceed by either the carbonyl oxygen atoms ('b_x-y_z' peptide fragmentation pathways)[3] or the N-terminus in its neutral form ('diketopiperazine' peptide fragmentation pathways).[3] Generation of b ions from CID of the CB[7]•FGGGG complex indicates that the b_x-y_z pathway is clearly operative because the diketopiperazine pathway yields mostly y ions.[3] Furthermore, the dominance of the b fragments from the doubly charged FGGGG complex indicates that only the b_x-y_z pathway is functional for the doubly charged complex ion. This seems to be due to the N-terminal amine of the ion retaining its charged form during CID. The two protons in the doubly charged complex would initially be located at the N-terminal amine and the carbonyl portal of CB[7] on the opposite side.[1] Among the two, the proton at the N-terminal amine would be better localized than the other due to both the N-terminal nitrogen and CB[7] stabilizing it. Therefore, the migrating proton would be the other proton, keeping the N-terminal charged during CID and blocking the diketopiperazine pathway. This process is summarized in Scheme S1.

By contrast, the diketopiperazine pathway is possible for the singly charged complex ion because the proton at the N-terminal is the only proton that can migrate, and its migration yields a neutral N-terminus. Although the b_x-y_z pathway can also generate y ions, the diketopiperazine pathway would bring CB[7] at the N-terminus closer to the charged fragmentation site, enabling its migration to the newly forming N-terminus (Scheme S2). The migration is possible because the N-terminal Phe can no longer form strong ion-dipole interactions with CB[7], and the interaction between the side chain of Phe and CB[7] is not very strong in the gas phase.[1] The

fragmentation mechanism suggested for the CB[7]•FGGGG complex can also be applied to the CB[7]•KGGGG complex because their fragmentation pathways are similar; the doubly charged form shows the dominance of the b ions, and only its singly charged form generates y ions with CB[7]. To summarize, fragmentation of the CB[7]•peptide complexes can be explained by the typical fragmentation pathways involving proton transfer to the amide backbone. Additionally, it is possible that CB[7] migrates during the CID process.

Mutation Studies of InsB1-11 Peptides. To understand the fragmentation pathways and the structures of CB[7]-bound peptide ions, we performed mutation studies of InsB1-11 peptides. Three amidated peptides were prepared, i.e., FVNQHLCGSHL-NH_2 (WT-NH_2), FVNQALCGSHL-NH_2 (H5A), and FVNQHLCGSAL-NH_2 (H10A). The designation "-NH_2" indicates a C-terminal primary amide due to their synthesis on Rink amide resin. In all cases, the peptide ions bound to CB[7] show richer fragmentation patterns than those in the absence of CB[7], thus confirming the utility of CB[7] in enhancing fragmentation (Figure S12). An interesting observation is the significant suppression of y-type ions upon mutation of His10 to Ala (Figure S12c). This observation suggests that the presence of the charged His10 is important in the fragmentation process.

Figure S13a shows that both bare and complex ions of all three peptides display a single dominant peak in the ion mobility (IM) spectra. Two conformations are present for the H5A and H10A peptides, but the high-mobility (shorter arrival time) conformations correspond to the cysteine-bound covalent dimers, confirmed by their exact mass values and isotope patterns. Calibration of the arrival times provided

collision cross section (Ω_D) values, which are summarized in Table S7. It is observed that the +3 charged peptide ions with and without CB[7] have Ω_D values similar to the InsB1-11 peptide ions. Due to the removal of His, the dominant charge state for the H5A and H10A mutants are +2. The doubly charged H5A and H10A mutants exhibit small Ω_D values (263 $Å^2$ and 253 $Å^2$, respectively), indicating that their structures are more compact than those of the triply charged WT-NH_2 ion. This observation can be explained by a decrease in electrostatic repulsion upon charge reduction. Complexation of the doubly charged mutant peptides with CB[7] causes a significant increase in their Ω_D values to 355 $Å^2$ and 368 $Å^2$, which is expected owing to the addition of a large molecule (i.e. CB[7]) to a compact ion should increase the size of the ion.

Computational modeling of the mutant peptides with CB[7] yielded good agreement between the theoretical and experimental Ω_D values (Table S7). As is the case with the wild-type InsB1-11 peptide ion, CB[7] induces peptide tweezer structures in both WT-NH_2 and H5A ions, in which N-terminal Phe and His10 of the peptides interact simultaneously with the opposite portals of CB[7] (Figure S13b). However, in the case of the H10A complex ion, His5 and the N-terminal Phe are unable to interact simultaneously with the opposite portals of CB[7] due to the insufficient distance between them. This allows the positive charge on His5 to be solvated by intramolecular interactions with carbonyl oxygens of the peptide. Thus, these mutant experiments confirm that CB[7] most likely interacts with the N-terminal Phe and His10 in the wild-type peptide ion.

Figure S1. ESI mass spectra of peptic-digested InsB without CB[7] (top), and with CB[7] (bottom).

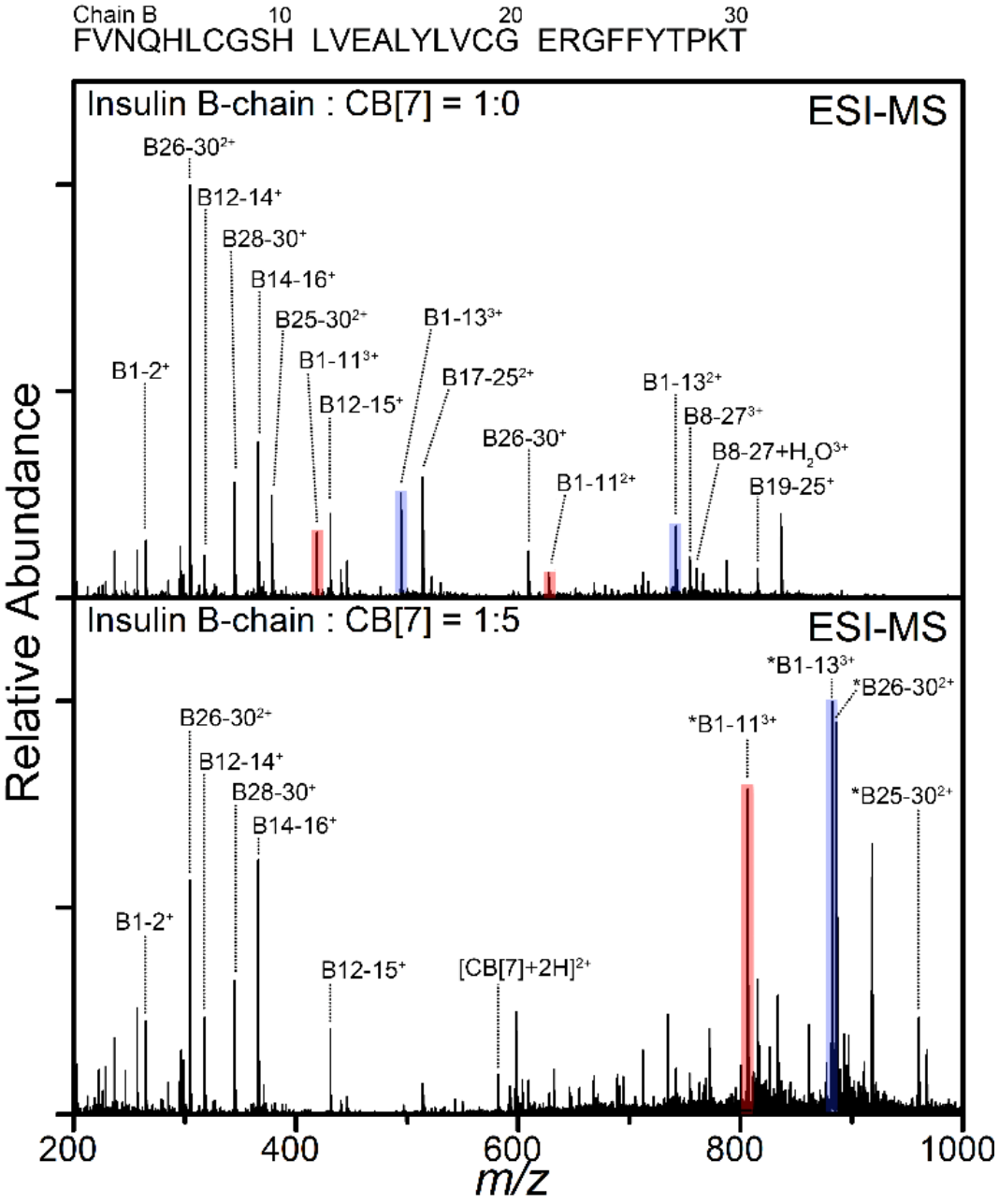

Figure S2. ESI mass spectra of peptic-digested Ins without CB[7] (top), and with CB[7] (bottom).

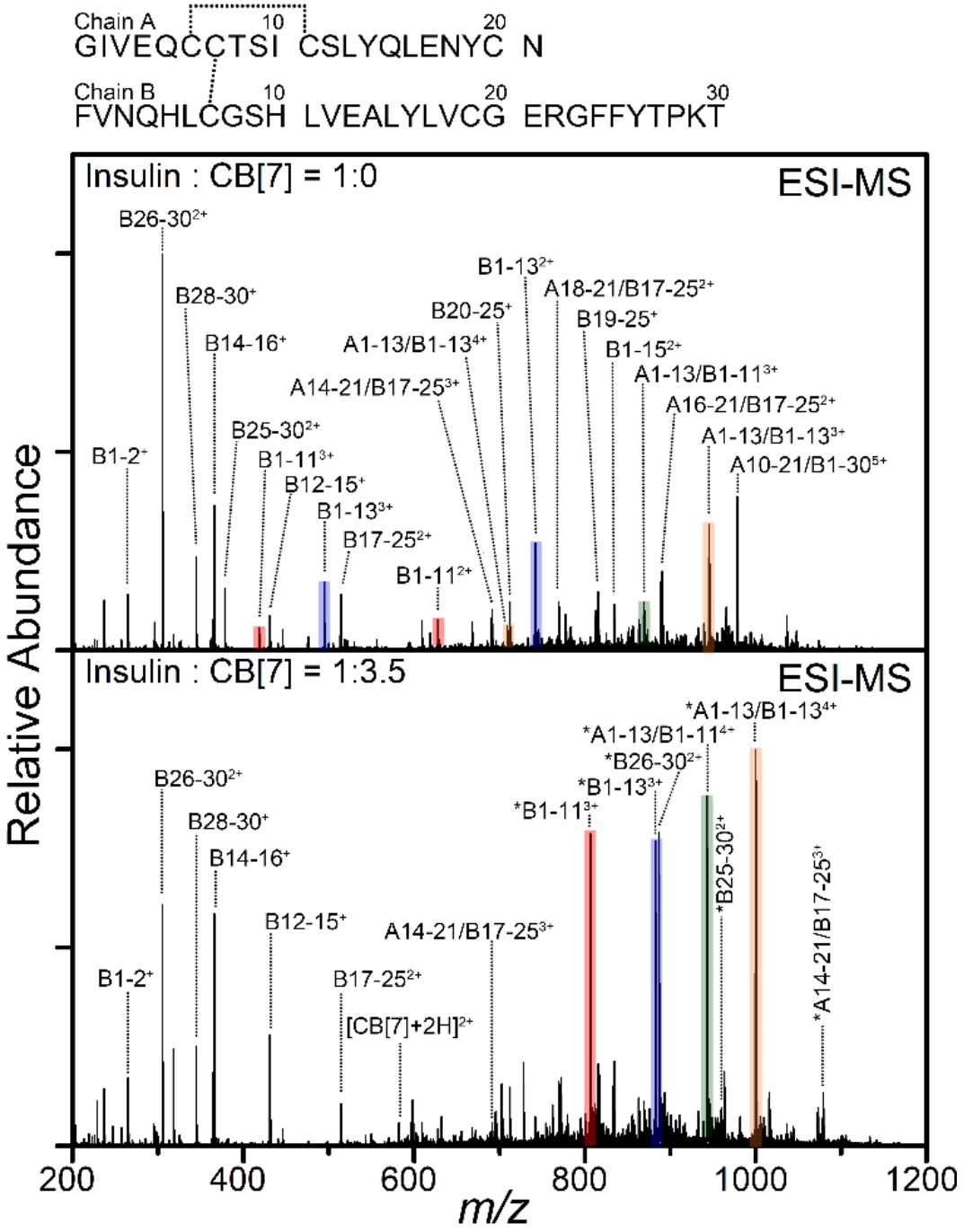

Figure S3. ESI mass spectra of peptic-digested Ubq without CB[7] (top), and with CB[7] (bottom).

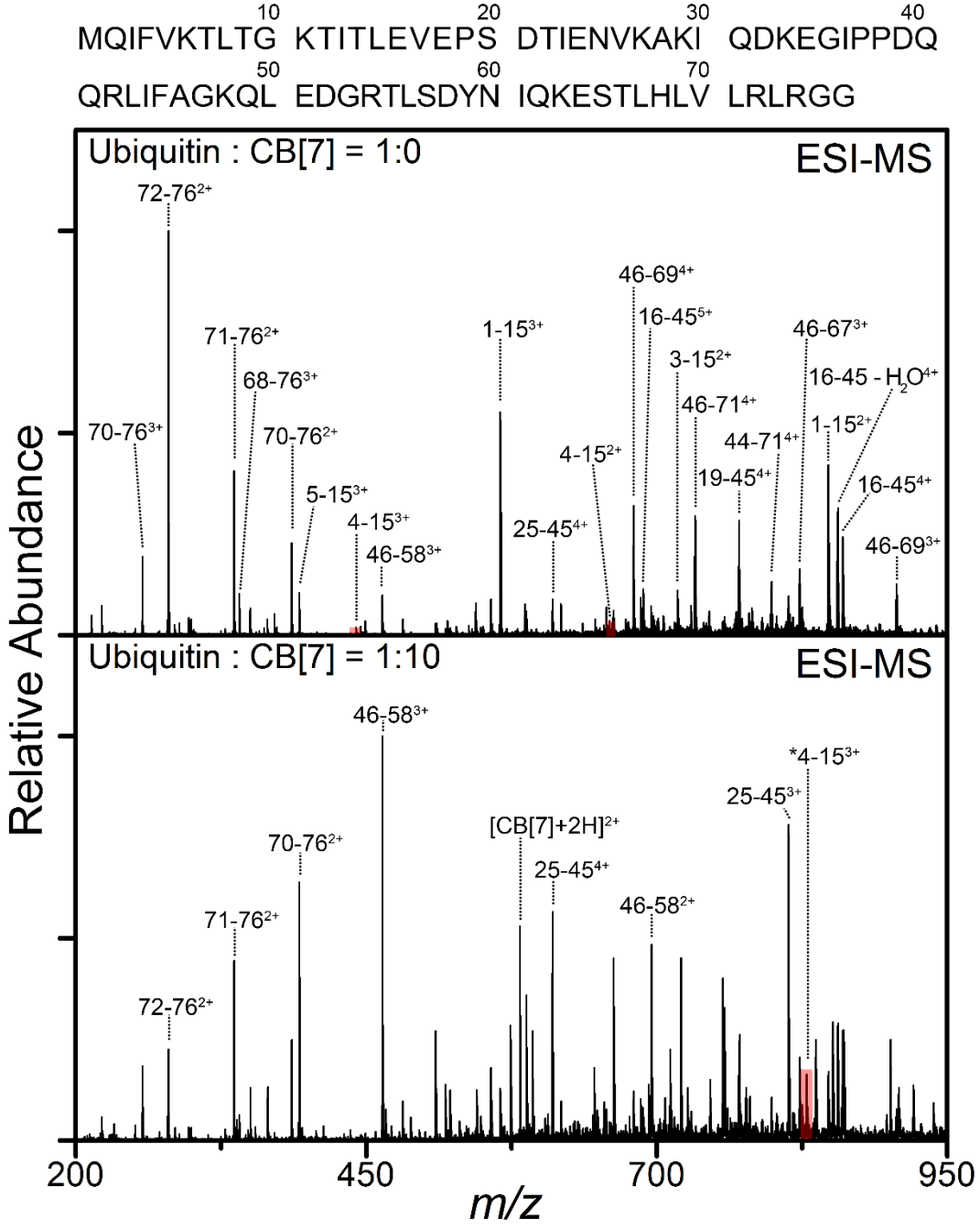

Figure S4. ESI mass spectra of peptic-digested Myb without CB[7] (top), and with CB[7] (bottom).

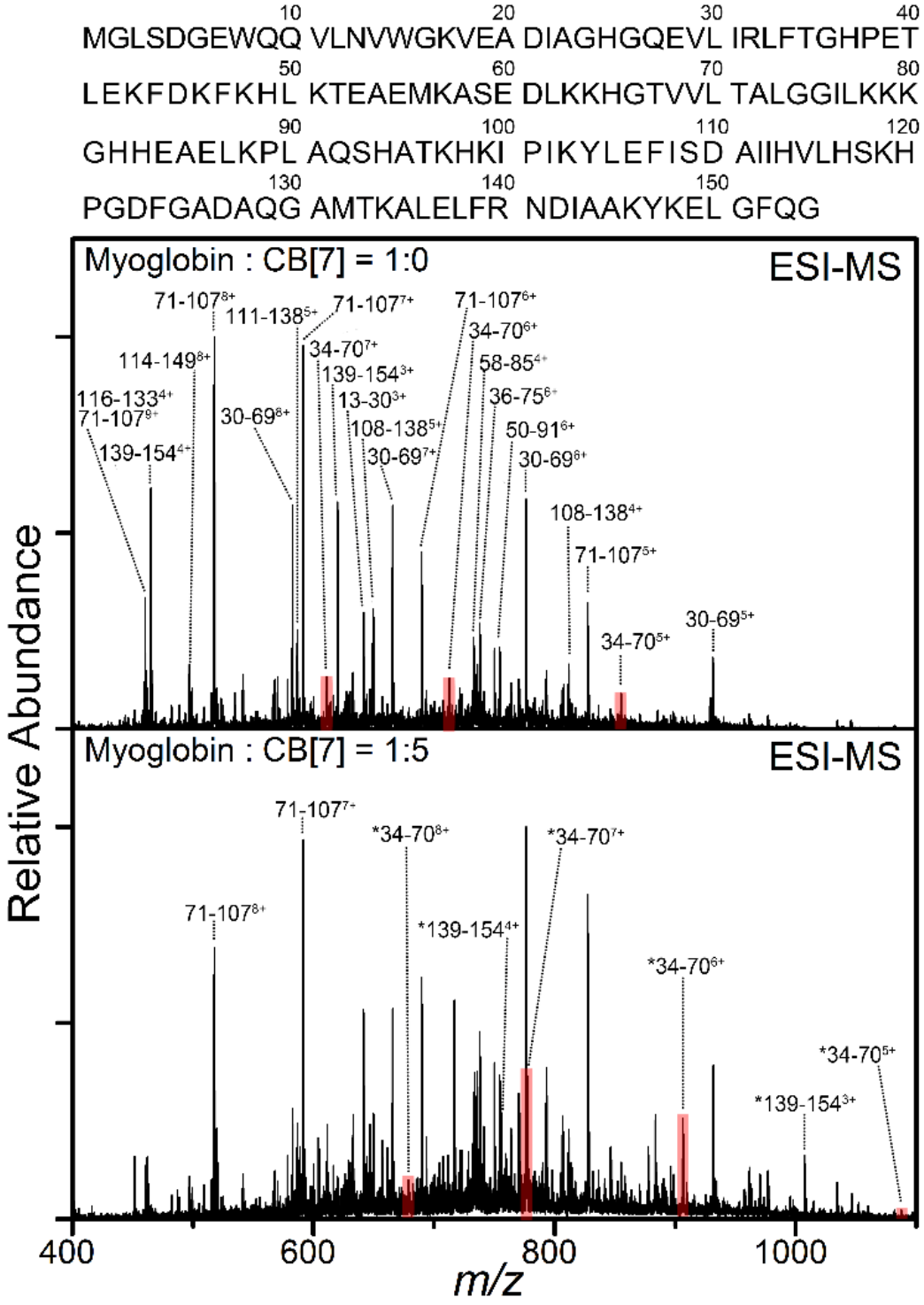

Table S1. Peptides from the peptic digestion of InsB.

Monoisotopic *m/z* (charge state)	Sequence	Residue	Expected mass	Δ
265.01 (+1)	FV	B1-2	265.15	-0.15
305.06 (+2)	YTPKT	B26-30	609.32	-0.22
318.05 (+1)	VEA	B12-14	318.17	-0.11
345.11 (+1)	PKT	B28-30	345.21	-0.11
366.10 (+1)	ALY	B14-16	366.20	-0.11
378.59 (+2)	FYTPKT	B25-30	756.39	-0.22
418.77 (+3)	FVNQHLCGSHL	B1-11	1254.60	-0.33
431.14 (+1)	VEAL	B12-15	431.25	-0.11
494.81 (+3)	FVNQHLCGSHLVE	B1-13	1482.72	-0.31
514.15 (+2)	LVCGERGFF	B17-25	1027.50	-0.21
609.24 (+1)	YTPKT	B26-30	609.32	-0.09
627.81 (+2)	FVNQHLCGSHL	B1-11	1254.60	-0.19
741.78 (+2)	FVNQHLCGSHLVE	B1-13	1482.72	-0.16
754.27 (+3)	GSHLVEALYLVCGERGFFYT	B8-27	2261.11	-0.30
760.29 (+3)	GSHLVEALYLVCGERGFFYT+H_2O	B8-27	2261.11	-0.27
815.30 (+1)	CGERGFF	B19-25	815.35	-0.06

Table S2. Peptides from the peptic digestion of Ins.

Monoisotopic *m/z* (charge state)	Sequence	Residue	Expected mass	Δ
265.12 (+1)	FV	B1-2	265.15	-0.03
305.17 (+2)	YTPKT	B26-30	609.32	0.02
345.22 (+1)	PKT	B28-30	345.21	0.01
366.21 (+1)	ALY	B14-16	366.20	0.01
378.71 (+2)	FYTPKT	B25-30	756.39	0.02
418.88 (+3)	FVNQHLCGSHL	B1-11	1254.60	0.01
431.26 (+1)	VEAL	B12-15	431.25	0.01
494.92 (+3)	FVNQHLCGSHLVE	B1-13	1482.72	0.03
514.26 (+2)	LVCGERGFF	B17-25	1027.50	0.01
627.81 (+2)	FVNQHLCGSHL	B1-11	1254.60	0.01
690.98 (+3)	YQLENYCN/LVCGERGFF	A14-21/B17-25	2070.88	0.05
709.09 (+4)	GIVEQCCTSICSL/FVNQHLCGSHLVE	A1-13/B1-13	2833.26	0.06
712.34 (+1)	GERGFF	B20-25	712.34	0.00
741.88 (+2)	FVNQHLCGSHLVE	B1-13	1482.72	0.03
769.35 (+2)	NYCN/LVCGERGFF	A18-21/B17-25	1537.63	0.06
815.39 (+1)	CGERGFF	B19-25	815.35	0.04
833.88 (+2)	FVNQHLCGSHLVEAL	B1-15	1666.79	-0.05
869.08 (+3)	GIVEQCCTSICSL/FVNQHLCGSHL	A1-13/B1-11	2605.15	0.08
890.42 (+2)	LENYCN/LVCGERGFF	A16-21/B17-25	1779.76	0.06
945.14 (+3)	GIVEQCCTSICSL/FVNQHLCGSHLVE	A1-13/B1-13	2833.26	0.15
978.45 (+5)	ICSLYQLENYCN/FVNQHLCGSHLVEALYLVCGERGFFYTPKT	A10-21/B1-30	4885.17	-0.02

Table S3. Peptides from the peptic digestion of Ubq.

Monoisotopic *m/z* (charge state)	Sequence	Residue	Expected mass	Δ
257.49 (+3)	VLRLRGG	70-76	770.50	-0.04
279.67 (+2)	RLRGG	72-76	558.35	-0.02
336.20 (+2)	LRLRGG	71-76	671.43	-0.04
340.87 (+3)	HLVLRLRGG	68-76	1020.64	-0.04
385.74 (+2)	VLRLRGG	70-76	770.50	-0.03
392.23 (+3)	VKTLTGKTITL	5-15	1174.74	-0.07
441.25 (+3)	FVKTLTGKTITL	4-15	1321.81	-0.08
463.89 (+3)	AGKQLEDGRTLSD	46-58	1389.70	-0.06
565.32 (+3)	MQIFVKTLTGKTITL	1-15	1693.99	-0.07
610.07 (+4)	NVKAKIQDKEGIPPDQQRLIF	25-45	2437.28	-0.04
661.37 (+2)	FVKTLTGKTITL	4-15	1321.81	-0.08
679.83 (+4)	AGKQLEDGRTLSDYNIQKESTLHL	46-69	2716.39	-0.11
688.14 (+5)	EVEPSDTIENVKAKIQDKEGIPPDQQRLIF	16-45	3436.80	-0.15
717.91 (+2)	IFVKTLTGKTITL	3-15	1434.89	-0.08
732.86 (+4)	AGKQLEDGRTLSDYNIQKESTLHLVL	46-71	2928.54	-0.13
770.64 (+4)	PSDTIENVKAKIQDKEGIPPDQQRLIF	19-45	3079.64	-0.12
797.89 (+4)	IFAGKQLEDGRTLSDYNIQKESTLHLVL	44-71	3188.70	-0.16
822.72 (+3)	AGKQLEDGRTLSDYNIQKESTL	46-67	2466.25	-0.11
847.46 (+2)	MQIFVKTLTGKTITL	1-15	1693.99	-0.08
855.42 (+4)	EVEPSDTIENVKAKIQDKEGIPPDQQRLIF-H_2O	16-45	3436.80	-0.15
859.91 (+4)	EVEPSDTIENVKAKIQDKEGIPPDQQRLIF	16-45	3436.80	-0.19
906.09 (+3)	AGKQLEDGRTLSDYNIQKESTLHL	46-69	2716.39	-0.13

Table S4. Peptides from the peptic digestion of Myb.

Monoisotopic *m/z* (charge state)	Sequence	Residue	Expected mass	Δ
288.19 (+1)	IR	31-32	288.20	-0.02
334.15 (+1)	ISD	108-110	334.16	-0.01
460.03 (+9)	TALGGILKKKGHHEAELKPLAQSHATKHKIPIKYLEF	71-107	4132.35	-0.21
460.72 (+4)	LHSKHPGDFGADAQGAMT	116-133	1839.84	0.00
462.23 (+2)	IAGHGQEVL	22-30	923.49	-0.04
464.98 (+4)	FRNDIAAKYKELGFQG	139-154	1856.97	-0.08
466.04 (+10)	LIRLFTGHPETLEKFDKFKHLKTEAEMKASEDLKKHGTVV	30-69	4651.51	-0.16
496.64 (+8)	HVLHSKHPGDFGADAQGAMTKALELFRNDIAAKYKE	114-149	3966.01	0.07
499.02 (+8)	TALGGILKKKGHHEAELKPLAQSHATKHKIPIKYLE	71-106	3985.29	-0.17
517.41 (+8)	TALGGILKKKGHHEAELKPLAQSHATKHKIPIKYLEF	71-107	4132.35	-0.18
519.74 (+2)	DIAGHGQEVL	21-30	1038.52	-0.04
541.26 (+6)	ISDAIIHVLHSKHPGDFGADAQGAMTKALEL	108-138	3242.66	-0.13
567.88 (+7)	LTALGGILKKKGHHEAELKPLAQSHATKHKIPIKYL	70-105	3969.33	-0.19
570.61 (+2)	AKYKELGFQG	145-154	1140.60	-0.40
578.28 (+5)	IPIKYLEFISDAIIHVLHSKHPGDF	100-124	2889.57	-2.19
582.31 (+8)	LIRLFTGHPETLEKFDKFKHLKTEAEMKASEDLKKHGTVV	30-69	4651.51	-0.14
586.29 (+5)	AIIHVLHSKHPGDFGADAQGAMTKALEL	111-138	2927.52	-0.12
591.19 (+7)	TALGGILKKKGHHEAELKPLAQSHATKHKIPIKYLEF	71-107	4132.35	-0.11
610.74 (+7)	FTGHPETLEKFDKFKHLKTEAEMKASEDLKKHGTVVL	34-70	4269.24	-0.14
619.65 (+3)	FRNDIAAKYKELGFQG	139-154	1856.97	-0.05
632.47 (+7)	GHPETLEKFDKFKHLKTEAEMKASEDLKKHGTVVLTALGG	36-75	4420.33	0.91
641.32 (+3)	NVWGKVEADIAGHGQEVL	13-30	1921.98	-0.04
646.50 (+7)	LKTEAEMKASEDLKKHGTVVLTALGGILKKKGHHEAELKPLA	50-91	4519.54	-0.13
649.32 (+5)	ISDAIIHVLHSKHPGDFGADAQGAMTKALEL	108-138	3242.66	-0.09
665.34 (+7)	LIRLFTGHPETLEKFDKFKHLKTEAEMKASEDLKKHGTVV	30-69	4651.51	-0.16
689.55 (+6)	TALGGILKKKGHHEAELKPLAQSHATKHKIPIKYLEF	71-107	4132.35	-0.12
712.36 (+6)	FTGHPETLEKFDKFKHLKTEAEMKASEDLKKHGTVVL	34-70	4269.24	-0.11
721.38 (+6)	DKFKHLKTEAEMKASEDLKKHGTVVLTALGGILKKKGHH	45-83	4323.41	-0.16
735.41 (+4)	ASEDLKKHGTVVLTALGGILKKKGHHEA	58-85	2937.66	0.93
737.71 (+6)	GHPETLEKFDKFKHLKTEAEMKASEDLKKHGTVVLTALGG	36-75	4420.33	0.86
754.06 (+6)	LKTEAEMKASEDLKKHGTVVLTALGGILKKKGHHEAELKPLA	50-91	4519.54	-0.24
763.93 (+4)	ILKKKGHHEAELKPLAQSHATKHKIPI	76-102	3052.79	-0.10
770.22 (+5)	GKVEADIAGHGQEVLIRLFTGHPETLEKFDKFKH	16-49	3847.03	0.06
776.07 (+6)	LIRLFTGHPETLEKFDKFKHLKTEAEMKASEDLKKHGTVV	30-69	4651.51	-0.14
792.84 (+5)	GKVEADIAGHGQEVLIRLFTGHPETLEKFDKFKHL	16-50	3960.11	0.04
805.41 (+1)	MTKALEL	132-138	805.45	-0.04
811.40 (+4)	ISDAIIHVLHSKHPGDFGADAQGAMTKALEL	108-138	3242.66	-0.08
827.25 (+5)	TALGGILKKKGHHEAELKPLAQSHATKHKIPIKYLEF	71-107	4132.35	-0.14
854.64 (+5)	FTGHPETLEKFDKFKHLKTEAEMKASEDLKKHGTVVL	34-70	4269.24	-0.10
931.09 (+5)	LIRLFTGHPETLEKFDKFKHLKTEAEMKASEDLKKHGTVV	30-69	4651.51	-0.11

Figure S5. Low-energy CID (ESI-MS^2) spectra of (a) the InsB1-13 peptide ion, and (b) the InsA1-13/B1-13 peptide ion, without CB[7] (top), and with CB[7] (bottom).

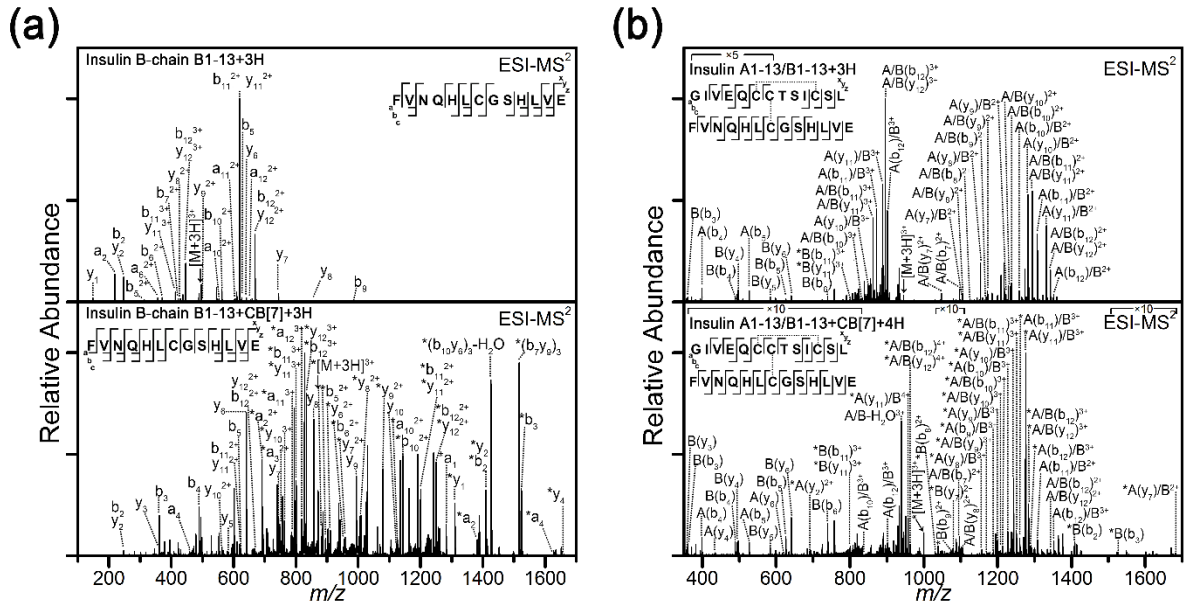

Figure S6. MALDI mass spectra of peptic-digested InsB without CB[7] (top), and with CB[7] (bottom).

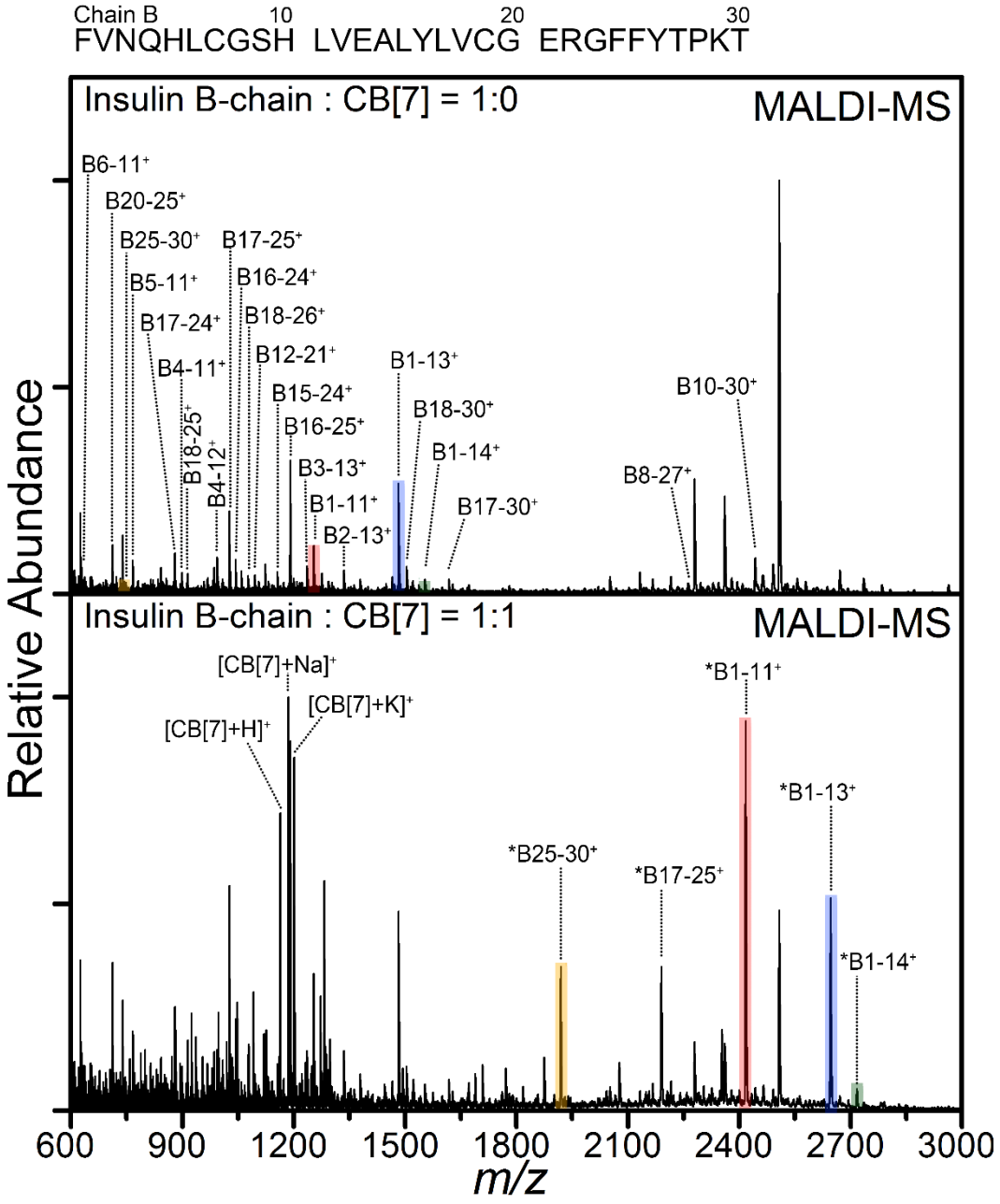

Figure S7. MALDI mass spectra of peptic-digested Ubq without CB[7] (top), and with CB[7] (bottom).

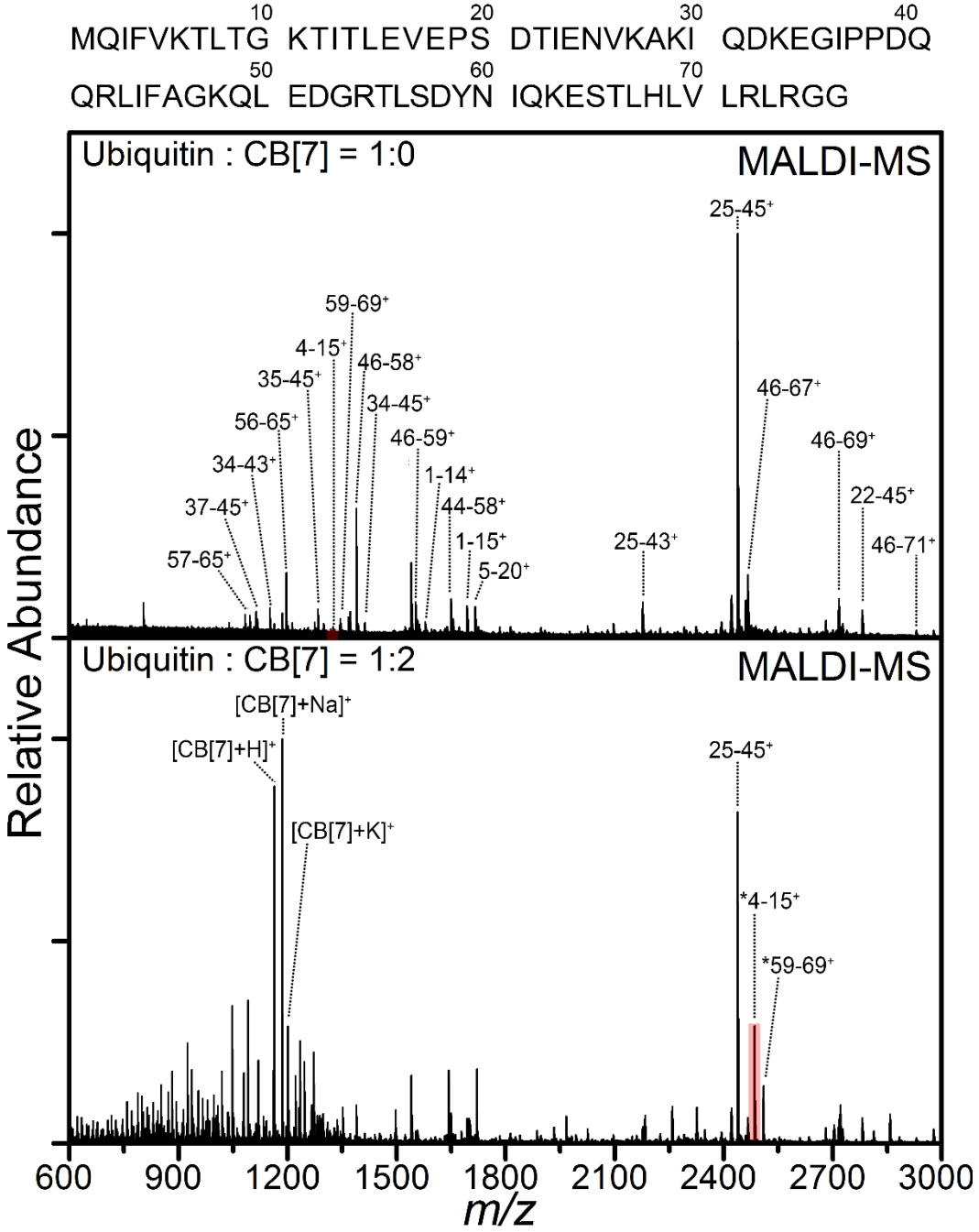

Table S5. Ratios of the relative abundances (RAs) of peptide peaks in the presence and the absence of CB[7], in MALDI-MS.

Protein	Sequence (residue)	Peptide *m/z* (charge state)	CB[7]-peptide complex *m/z* (charge state)	RA ratio
InsB	FVNQHLCGSHL (1-11)	1254.60 (+1)	1919.87 (+1)	8.03
	FVNQHLCGSHLVE (1-13)	1482.77 (+1)	2418.11 (+1)	1.92
	FVNQHLCGSHLVEA (1-14)	1553.78 (+1)	2646.31 (+1)	1.51
	FYTPKT (25-30)	*	2717.30 (+1)	*
Ubq	FVKTLTGKTITL (4-15)	*	2485.43 (+1)	*

*Not observed without the addition of CB[7]

Figure S8. Low-energy CID (MALDI-MS^2) spectra of (a) the InsB1-11 peptide ion, and (b) the Ubq4-15 peptide ion, in complex with CB[7].

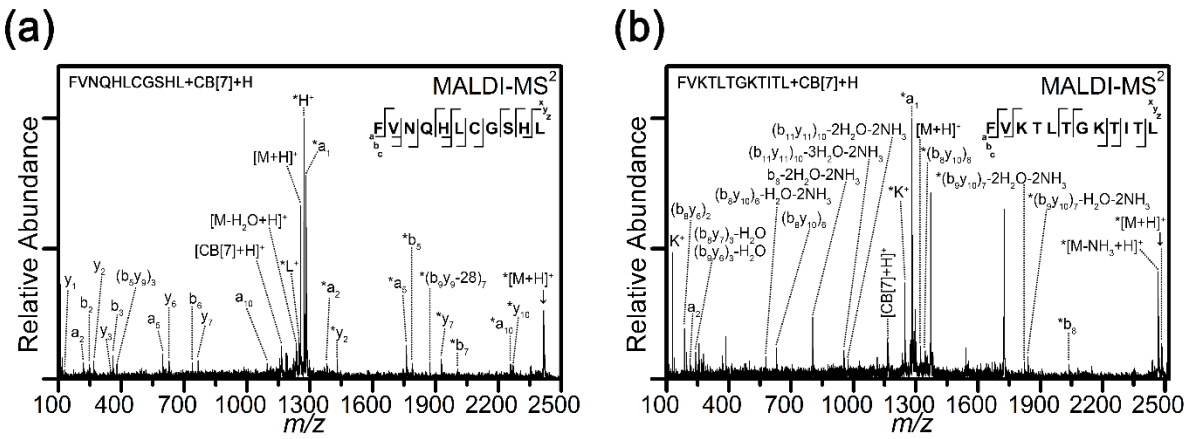

Figure S9. ESI mass spectra and low-energy CID (ESI-MS^2) spectra of (a) FGGGG, and (b) KGGGG peptides, with CB[7].

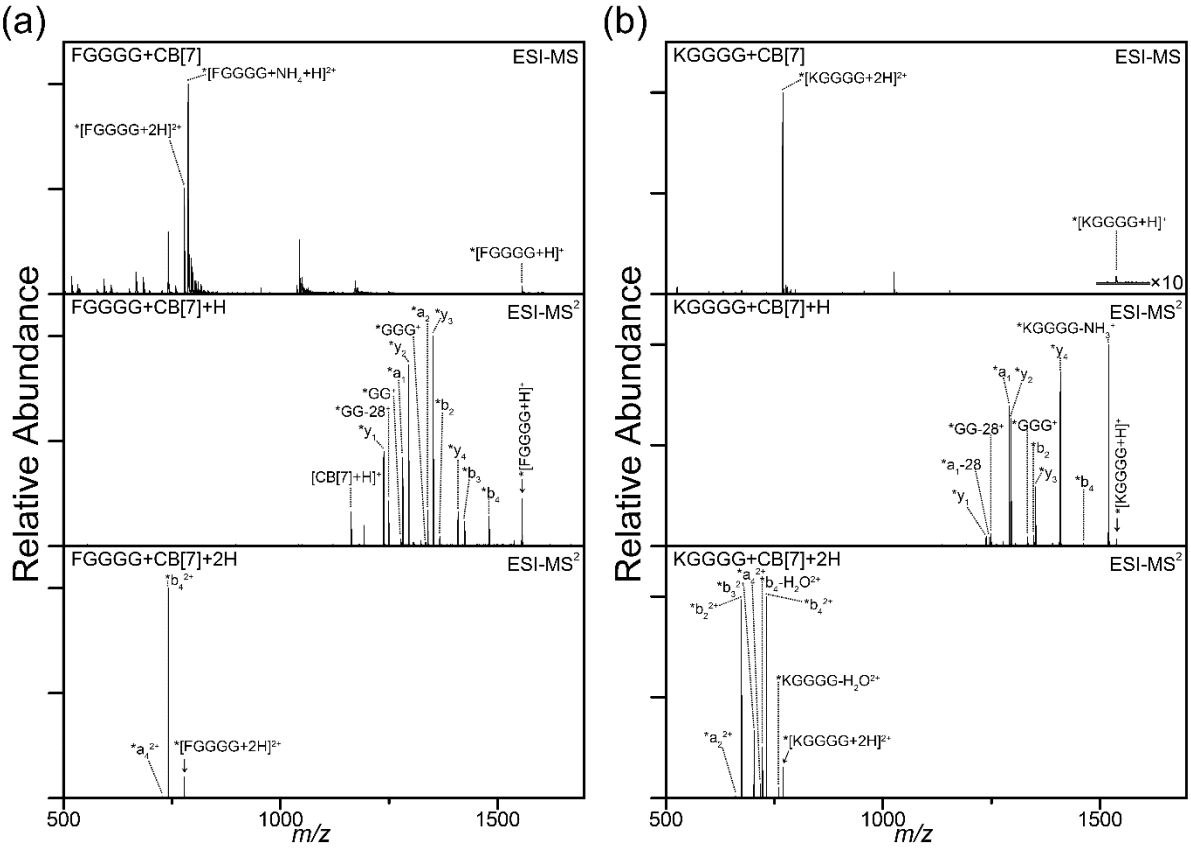

Scheme S1. Proposed fragmentation pathway of doubly charged CB[7]-FGGGG complex ions.

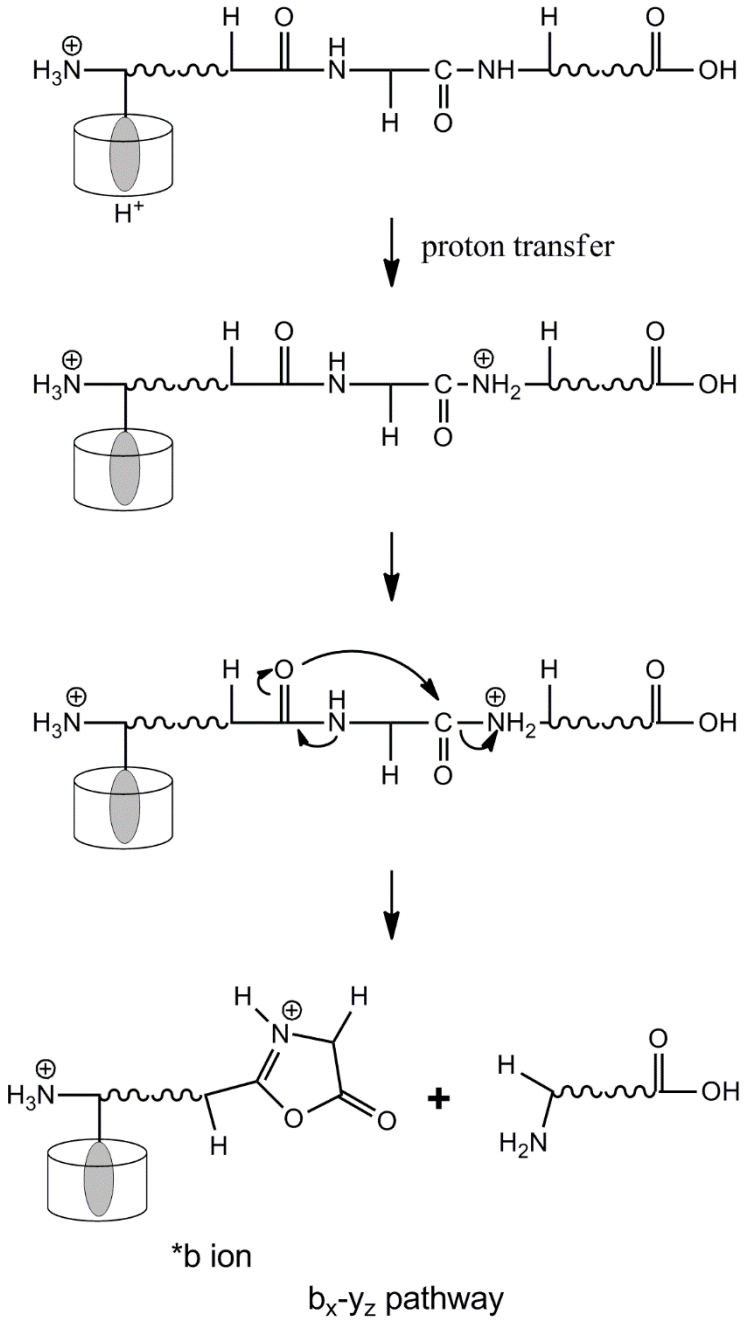

Scheme S2. Proposed fragmentation pathway of singly charged CB[7]-FGGGG complex ions.

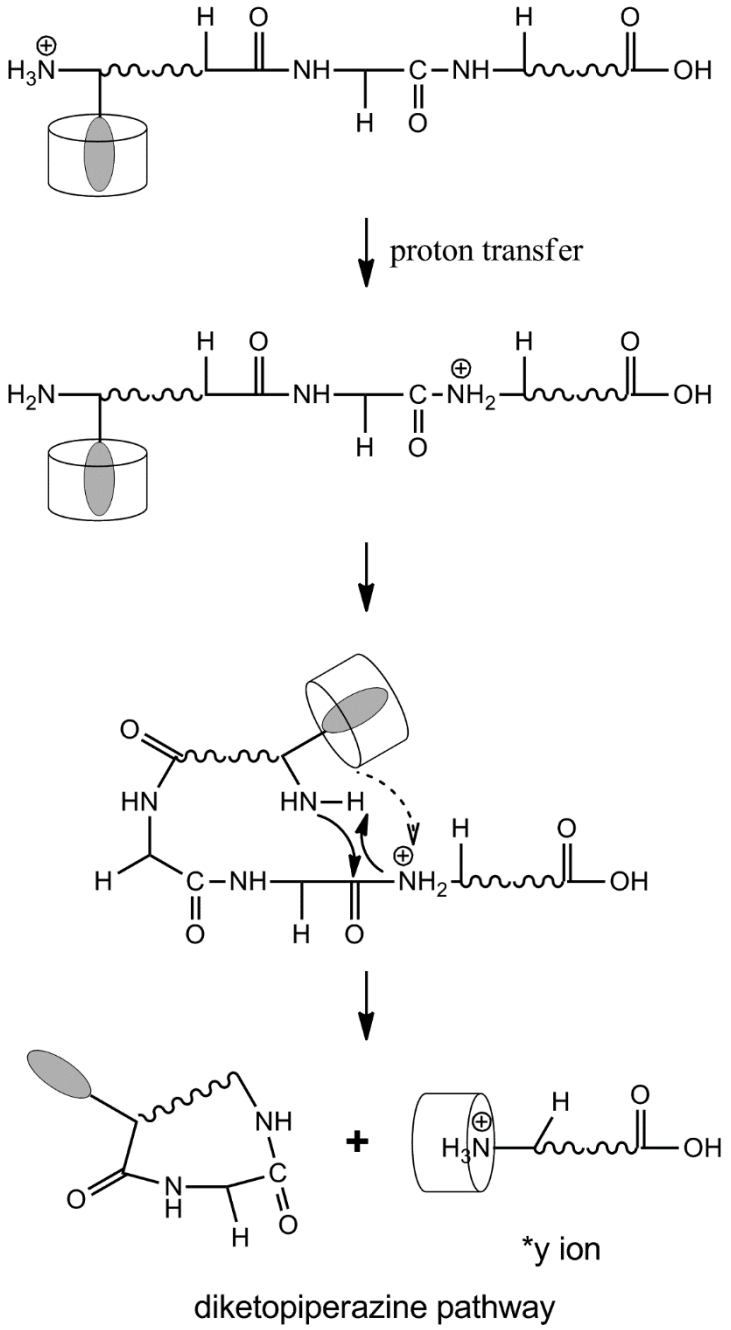

Figure S10. Ion mobility spectra of (a) the InsB1-11 peptide ion, (b) the InsB1-13 peptide ions, (c) the InsA1-13/B1-11 peptide ion, (d) the InsA1-13/B1-13 peptide ion, and (e) the Ubq4-15 peptide ion, without (top), and with (bottom) CB[7]. Small, non-dominant peaks in the spectra arise from noise and less abundant overlapping ions.

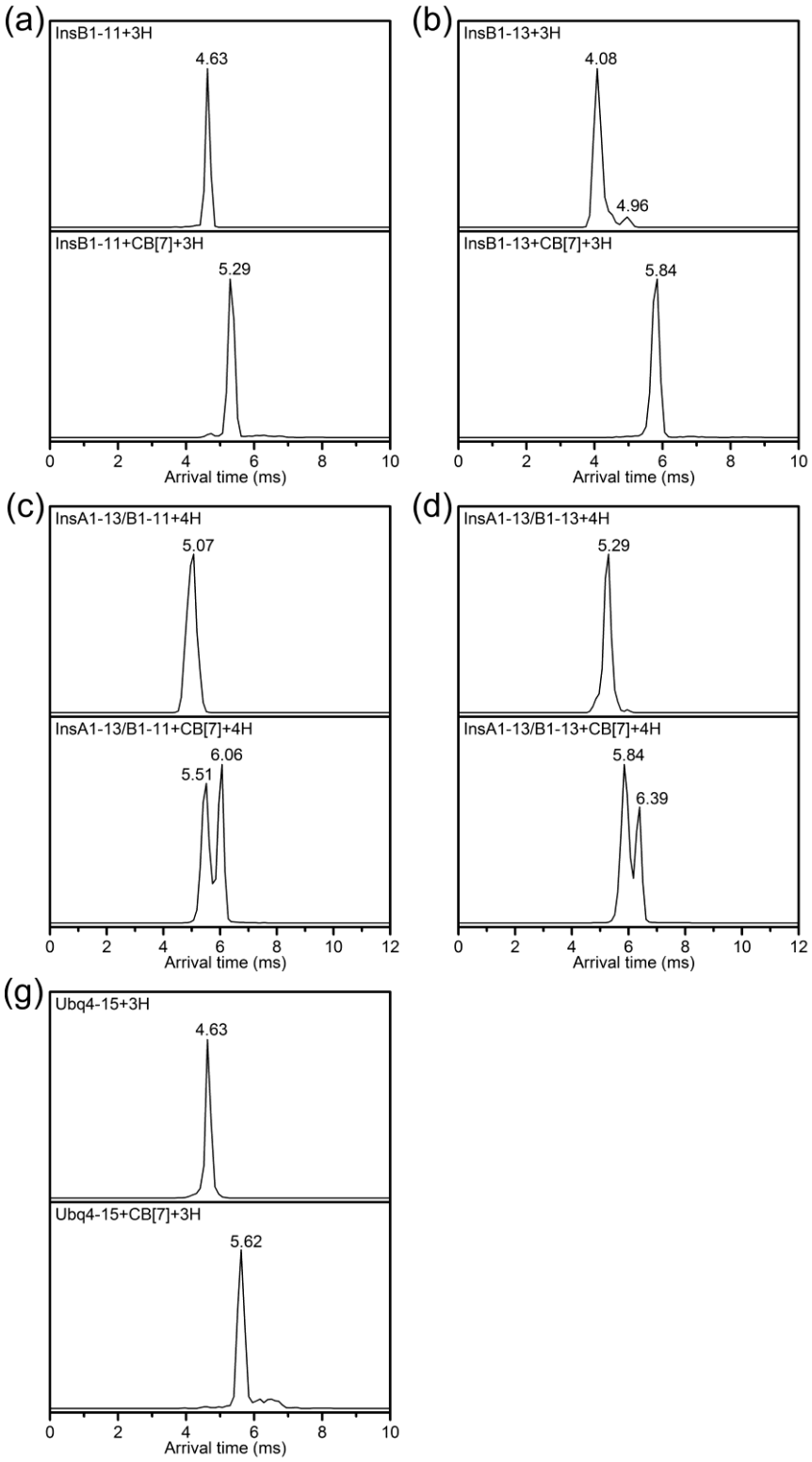

Table S6. Experimental and theoretical collision cross-section (Ω_D) values of peptide ions and peptide complex ions. The experimental values are averages from three experiments, and the theoretical values are averages of five lowest-energy structures. The errors are standard deviations.

Protein	Ion	Experimental Ω_D (Å^2)	Theoretical Ω_D (Å^2)	Error (%)
InsB	FVNQHLCGSHL^{3+} (1-11)	315 ± 4	-	-
	FVNQHLCGSHLVE^{3+} (1-13)	286 ± 5 337 ± 6	-	-
	*FVNQHLCGSHL^{3+} (1-11)	347 ± 3	360 ± 4	+3.6
	*FVNQHLCGSHLVE^{3+} (1-13)	373 ± 5	385 ± 5	+3.2
Ins	GIVEQCCTSICSL/FVNQHLCGSHL^{4+} (A1-13/B1-11)	449 ± 5	-	-
	GIVEQCCTSICSL/FVNQHLCGSHLVE^{4+} (A1-13/B1-13)	462 ± 4	-	-
	*GIVEQCCTSICSL/FVNQHLCGSHL^{4+} (A1-13/B1-11)	474 ± 3 512 ± 8	528 ± 18	+3.1
	*GIVEQCCTSICSL/FVNQHLCGSHLVE^{4+} (A1-13/B1-13)	500 ± 8 529 ± 7	547 ± 4	+3.4
Ubq	FVKTLTGKTITL^{3+} (4-15)	315 ± 4	-	-
	*FVKTLTGKTITL^{3+} (4-15)	364 ± 5	374 ± 5	+2.7

Figure S11. (a) The lowest-energy theoretical structures of InsB1-13, InsA1-13/B1-11, and InsA1-13/B1-13 peptides in complex with CB[7], with their theoretical Ω_D values as insets. (b) The lowest-energy theoretical structures of InsA1-13/B1-11 and InsA1-13/B1-13 whose theoretical Ω_D values agree with the experimental Ω_D (± 3%) of their high-mobility conformers (Figure S10).

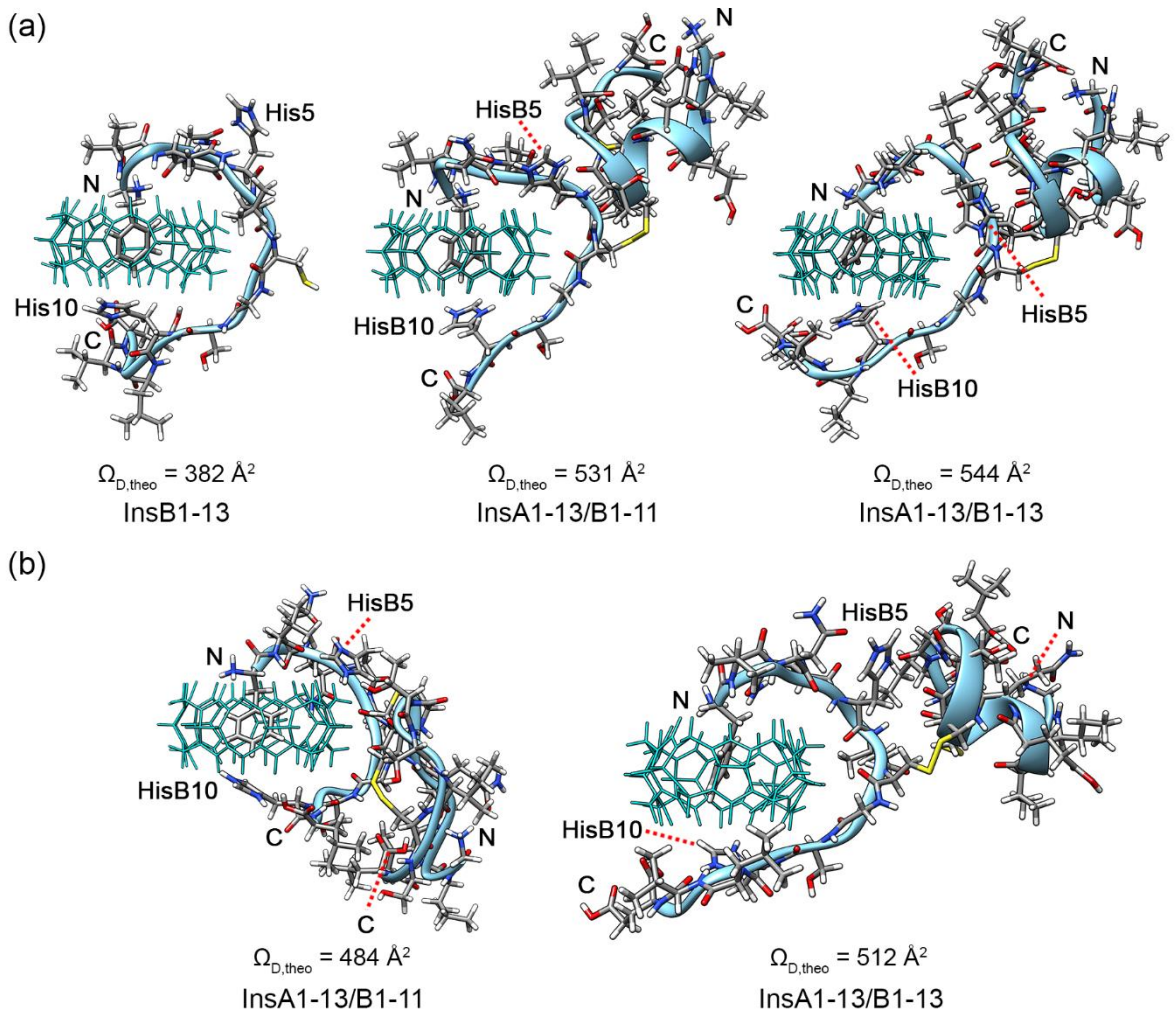

Figure S12. Low-energy CID (ESI-MS^2) spectra of (a) the WT-NH2 ion, (b) the H5A ion, and (c) the H10A ion, without CB[7] (top), and with CB[7] (bottom).

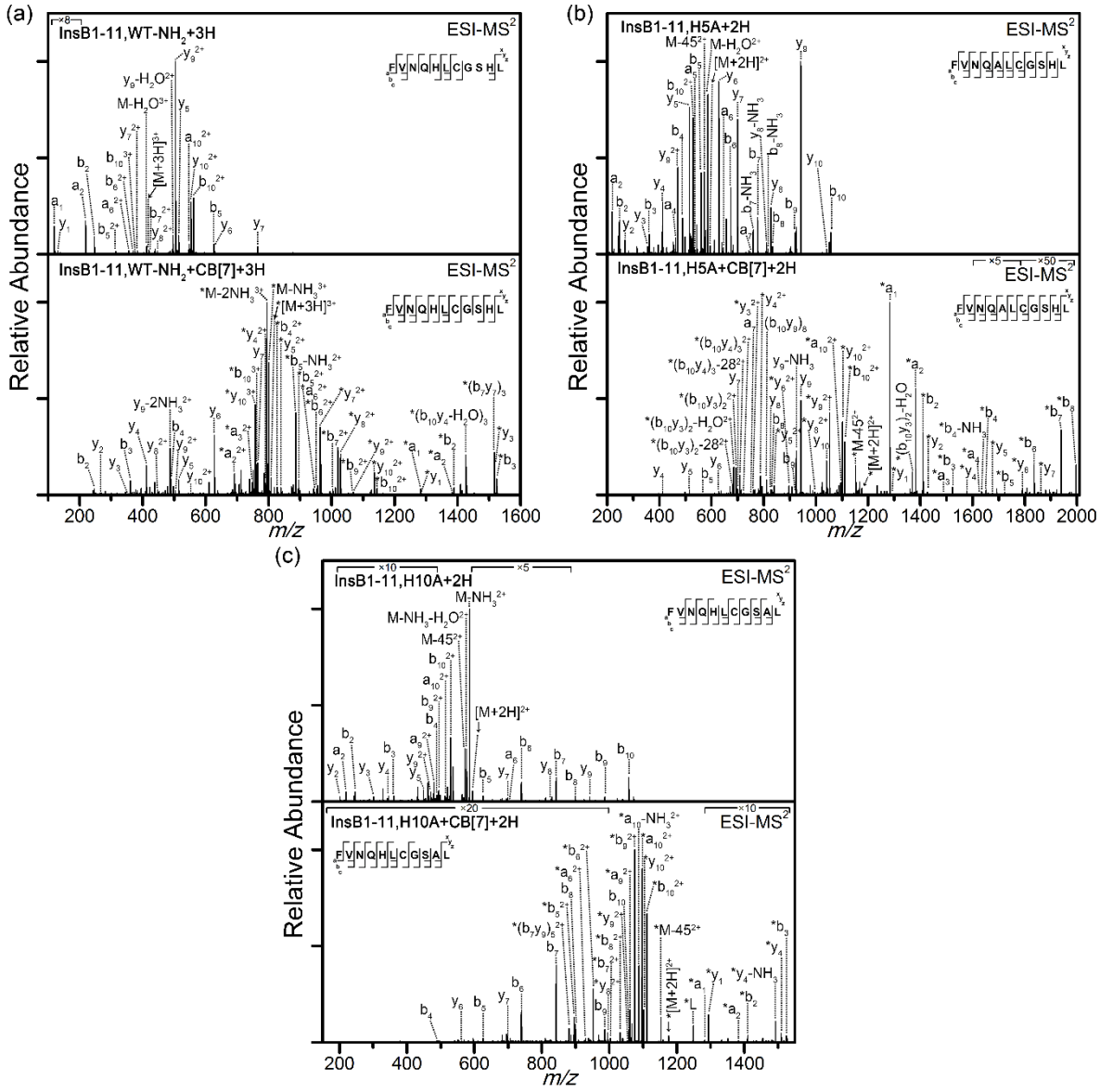

Figure S13. (a) Ion mobility spectra of the InsB1-11 mutants and their CB[7] complexes, and (b) the lowest-energy theoretical structures of the mutant complexes. 'M' and 'D' denote monomeric and dimeric ions, respectively.

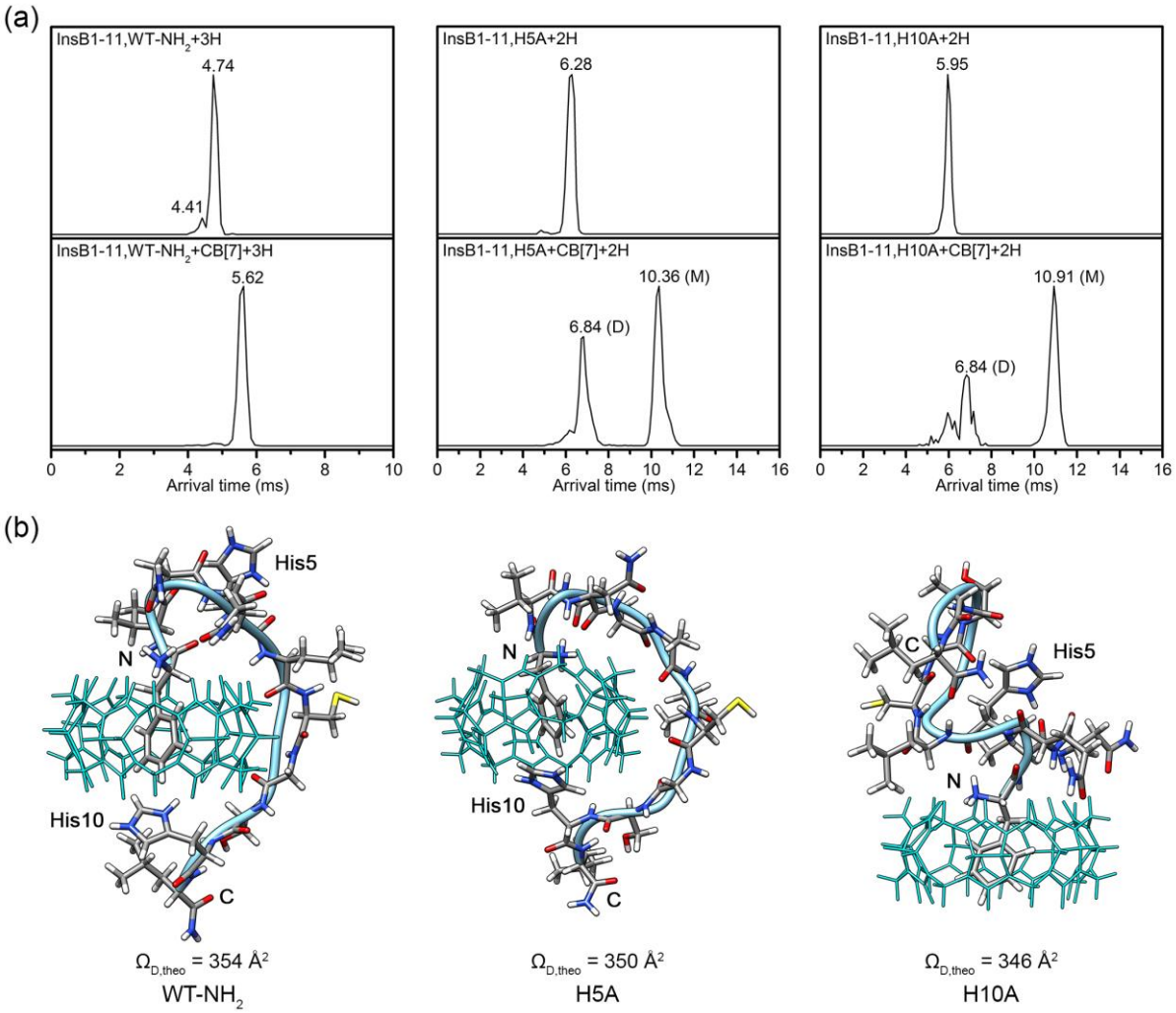

Table S7. Experimental and theoretical collision cross-section (Ω_D) values of mutated peptide ions and their complex ions

Peptide	Ion	Experimental Ω_D (Å^2)	Theoretical Ω_D (Å^2)	Error (%)
InsB1-11	FVNQHLCGSHL-$NH_2$$^{3+}$ (WT-NH_2)	323 ± 2	-	-
	FVNQALCGSHL-$NH_2$$^{2+}$ (H5A)	263 ± 5	-	-
	FVNQHLCGSAL-$NH_2$$^{2+}$ (H10A)	253 ± 3	-	-
	*FVNQHLCGSHL-$NH_2$$^{3+}$ (WT-NH_2)	363 ± 5	357 ± 5	-1.7
	*FVNQALCGSHL-$NH_2$$^{2+}$ (H5A)	355 ± 3	348 ± 8	-2.0
	*FVNQHLCGSAL-$NH_2$$^{2+}$ (H10A)	368 ± 3	345 ± 5	-6.3

REFERENCES

(1) Lee, J. W.; Lee, H. H. L.; Ko, Y. H.; Kim, K.; Kim, H. I. *J. Phys. Chem. B* **2015**, *119*, 4628-4636.
(2) Heath, B.; Jockusch, R. *J. Am. Soc. Mass. Spectrom.* **2012**, *23*, 1911-1920.
(3) Paizs, B.; Suhai, S. *Mass Spectrom. Rev.* **2005**, *24*, 508-548.
(4) Boyd, R.; Somogyi, A. *J. Am. Soc. Mass. Spectrom.* **2010**, *21*, 1275-1278.